Postsynthesis Crystallinity Improvement of Colloidal CdTe Nanoparticles Using Rapid Thermal Annealing

Steven A. Rutledge,[†] Abdiaziz A. Farah,[†] Jordan Dinglasan,[‡] Darren J. Anderson,[‡] Anjan Das,[‡] Jane Goh,[§] Cynthia Goh,[§] and Amr S. Helmy*[,†]

The Edward S. Rogers Sr. Department of Electrical and Computer Engineering, University of Toronto, 10 Kings College, Toronto, Ontario, M5S 3G4 Canada, Vive Nano Incorporated, 700 Bay Street, Suite 1100, Toronto, Ontario M5G 1Z6 Canada, and Department of Chemistry, University of Toronto, 80 St. George Street, Toronto, Ontario M5S 3H6 Canada

Received: July 02, 2009; Revised Manuscript Received: October 13, 2009

Rapid thermal annealing has been applied to poly(acrylic acid)-capped CdTe nanoparticles. This annealing process has shown to provide some control over the semiconductor core properties, while preserving the capping ligand intact. The photoluminescence and absorption properties of the nanoparticles remain nominally unchanged up to annealing temperatures of 400 °C and annealing durations of 30 s. This process was found to be an effective postsynthesis means of improving the crystallinity of the semiconductor core. The crystallinity enhancement is identified by solution-based Raman spectroscopy using a hollow-core photonic crystal fiber. This novel method of detecting a crystalline change in nanoparticles is corroborated by powder X-ray diffraction measurements and X-ray photoelectron spectroscopy.

Introduction

Colloidal nanoparticles (NPs) of numerous shapes, sizes, and compositions have been reported over the past two decades and continue to exhibit exciting optical and electrical characteristics.[1−4] In particular, CdTe semiconductor NPs have been demonstrated suitable for use in applications involving efficient solar cells,[5] ultrafast electron transfer,[6] and negative refractive index materials.[7] Significant progress in controlling the size and surface capping of wet chemically synthesized semiconducting NPs has also been achieved.[8] Water-soluble semiconducting NPs, such as CdTe, have been found useful as biological labels and for biomedical applications.[9] These nanoparticles require a high degree of structural and optical stability combined with a highly crystalline core for implementation into useful devices.[10] Such properties are often difficult to control during the initial growth procedure. Postsynthesis treatment to effectively manipulate NP characteristics is thus a highly sought after technique.

Postgrowth annealing to influence the crystallinity of colloidal NPs has been investigated with varying levels of success for colloidal NPs. However, the adiabatic nature and the time constants associated with oven annealing processes have been shown to diminish photoluminescence (PL) efficiency at temperatures below 200 °C.[11] Optical characteristics of colloidal NPs are significantly influenced by the surface ligand layer and its interaction with the semiconductor core.[12,13] Any postgrowth manipulation of these components of the colloidal NPs usually proves counterproductive from the applications stand point. The specific capping material used in this work is poly(acrylic acid) (PAA), which has a glass-transition temperature of 106 °C.[14] Above the glass-transition temperature, the polymer chains become much more mobile and could result in significant reorganization at the NP interface.[15] To maintain the attractive optical properties of the NPs, the mobility of the polymer ligands should be limited at temperatures sufficiently high to influence the crystalline properties of the semiconductor core. Although it is known that PAA is an insulating polymer and is not optimum for applications where carrier transport takes place, the demonstration of effective postsynthesis processing techniques that manipulate NP characteristics in this colloidal system with such a low glass-transition temperature serves as a valuable proof of concept. Influencing the semiconductor core, while maintaining the capping layer integrity, can be achieved via an isothermal annealing process with shorter annealing times than those possible in conventional oven annealing.

Technologically, this can be obtained via the use of rapid thermal annealing (RTA). RTA is a process in which an incoherent light source is incident uniformly on the sample, limiting thermal fluxes and resulting in a nonadiabatic heating mechanism. RTA has been applied extensively in semiconductor processing and has been demonstrated to provide numerous benefits in traditional semiconductor systems.[16] RTA has also been used to influence the photoluminescence (PL) efficiency, size dispersion, and compositional intermixing for epitaxial grown or implanted quantum dots (QDs).[17] However, its influence on the properties of polymer-capped nanostructures has not yet been investigated. If harnessed, the influence of RTA on colloidal nanostructures can present an attractive processing technique because the core material can be influenced while leaving the capping structure relatively unaffected. RTA has been recently shown to influence morphological and microstructural change on PEDOT-PSS thin films.[18] PEDOT-PSS films are often employed as a hole injection layer in polymer and quantum structured LEDs, and as such, the effects of this process on related systems, such as the QD layer, should be investigated as well.[19,20] In response to various external stimuli, water-soluble semiconducting QDs coated with organic polymers can undergo changes in surface properties via conformational changes of the protecting organic layer. This introduces

* To whom correspondence should be addressed. E-mail: a.helmy@utoronto.ca.
[†] The Edward S. Rogers Sr. Department of Electrical and Computer Engineering, University of Toronto.
[‡] Vive Nano Incorporated.
[§] Department of Chemistry, University of Toronto.

10.1021/jp9079475 CCC: $40.75
Published on Web 10/28/2009

new possibilities and avenues for self-assembly of more complex superstructures.[21−23] This study reports on the ability to influence the degree of crystallinity of polymer-stabilized CdTe NPs using RTA. Raman spectroscopy, PL, UV−visible absorption, X-ray photoelectron spectroscopy (XPS), and X-ray diffraction (XRD) have been utilized to analyze the crystallinity changes in the polymer-capped CdTe NPs.

Methods and Materials

The carboxylate-capped CdTe nanoparticles used in this study were provided by Vive Nano, Inc. and were synthesized in aqueous solution from Cd^{2+} collapsed high-molecular-weight poly(acrylic acid) and a tellurium source. First, 500 mL of $Cd(NO_3)_2$ solution (3 mM) was added dropwise to 500 mL of aqueous poly(acrylic acid) solution (2 mg/mL, 1.2×10^6 MW, pH adjusted to 6.8) under vigorous stirring (total 1 L). The solution was then exposed to a 254 nm UV lamp for approximately 2 h under continuous stirring. CdTe was synthesized by adding 25 mL of Na_2TeO_3 (10 mM), 1 g of solid sodium borohydride, and 1 g of solid trisodium citrate to the Cd/poly(acrylic acid) solution. The resulting solution was then refluxed for 4 h. After reflux, the solution was allowed to cool to room temperature. Thioacetamide solution (0.7 mL, 100 mM) was then added, and the solution was stirred and heated to 50 °C for another 18 h. The addition of the thioacetamide makes the nanoparticles more stable to ambient conditions. Without the addition of thioacetamide, the CdTe lose their fluorescence within 48 h. The solid carboxylate-capped CdTe was obtained by adding 50 mL of NaCl (3M) and 2000 mL of absolute ethanol to the 1 L solution. After a few minutes of stirring, solid CdTe precipitated from solution. The solid was then isolated via entrifugation and was washed with 70% ethanol three times. The isolated solid was air-dried and then stored in a desiccator before use.

Dried PAA-functionalized CdTe NPs are annealed in inert argon gas conditions for 30 s before a cooling off period. The annealing temperature ranges from 110 to 600 °C in 100 °C increments (110 °C is the minimum annealing temperature available) with the ramping temperature maintained at a constant 50 °C/s gradient in all cases. Two samples are used as controls: the unannealed NPs and the NPs undergoing the atmospheric processing conditions experienced in the RTA process (vacuum, followed by argon purge with no heat applied). All annealing is performed in an AnnealSys AS-One rapid thermal annealing system. The samples are then reweighed and dispersed in water to normalize NP concentrations of 2 mg/mL. All CdTe NPs are taken from the same processing batch that has been stored under refrigeration for several months. The optical properties of the unannealed NPs are found to be nominally constant over all annealing experiments, which took place over the course of 6 months. The comparable unannealed characteristics ensure that potential aging effects were negligible over the time span of the experiment. To rule out the presence of any metastable states after annealing, Raman spectroscopy and photoluminescence spectroscopy occurred days after the annealing process. The time delay between the optical measurements and other characterization methods was slightly greater due to the requirement that samples had to be analyzed externally. Raman scattering spectra were acquired using a Horiba Jobin Yvon HR800 integrated Raman system. Room temperature PL measurements were performed using a Tecan Safire system. UV−vis spectra of CdTe NP samples in aqueous solution were obtained using an Agilent 8453 UV−vis spectrometer. TEM is performed using a conventional Hitachi H-7000 electron microscope operating at 100 kV and 30 mA beam current. Samples for TEM were prepared by placing drops of a solution containing CdTe NPs on an amorphous carbon substrate supported by a copper grid and allowing the solvent to evaporate at room temperature. The powder X-ray diffraction measurements (p-XRD) were performed by a Rigaku Ultima III pXRD with a Cu Kα source (1.5418 Å), and Si powder is used as an internal standard. A Thermo Scientific Theta Probe XPS spectrometer (ThermoFisher, E. Grinstead, U.K.) is used for XPS analysis. The samples were measured in standard mode (i.e., all angle collected (60° angular acceptance)) for the survey spectra and the region spectra. A monochromatic Al Kα X-ray source is used, with a spot area of 300 μm. Charge compensation was provided utilizing the combined e^-/Ar^+ flood gun. The position of the energy scale was adjusted to place the main C 1s feature (C−C) at 285.0 eV. Peak areas were obtained from spectra run in low-resolution mode (pass energy = −200 eV). Elements of interest (C, Cd, and O were also measured in high-resolution mode (30 eV pass energy). The aforementioned analysis was not fully carried out for Te because of insufficient signal-to-noise ratio. However, the Te 3d peak was fitted because the separation of the oxide was more easily resolvable from the metal. The data processing was performed using the software *Avantage*, which was provided with the instrument.

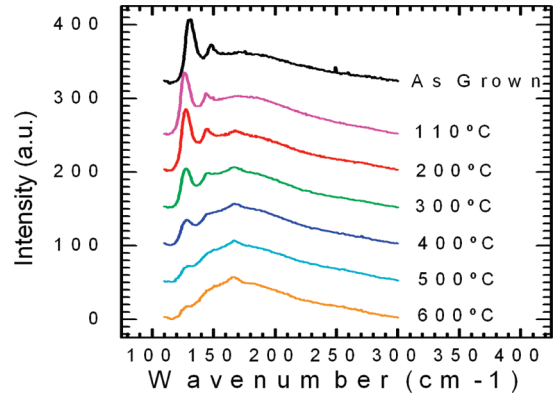

Figure 1. Raman spectra of annealed and as-grown NPs up to 600 °C.

Results and Discussion

The Raman properties of the NPs were studied first. This was carried out through a technique developed by Irizar et al.,[24] which uses a hollow-core photonic crystal fiber (HC-PCF) to copropagate the laser source in the liquid sample. With the enhanced sensitivity provided by this method, three Raman active peaks in the dispersed solution could be identified, as shown in Figure 1. These three peaks correspond to the Te A1 mode at ∼127 cm^{-1}, the Te E mode at ∼141 cm^{-1}, and the CdTe LO mode at ∼165 cm^{-1}.[25−27] Due to the modes' finite width and overlapping frequencies, there could also be a portion of the Te E peak contributed by the CdTe TO phonon mode that is located at ∼140 cm^{-1}. The presence of the two Te peaks has been attributed to Te inclusions within the center of the crystal or surface defects along the boundaries of the material.[25−27] It is not feasible to quantify from the Raman measurements the amount of Te inclusions or defects due to the fact that Te crystals exhibit a relatively high Raman scattering signal in comparison to CdTe as a result of unequal Raman cross sections.[26,28] Following a baseline correction and peak fitting, Gaussian−Lorentzian peaks were fitted to the Raman spectra for analysis. Figure 2 shows a reduction in the intensity ratios of the Te phonon peaks

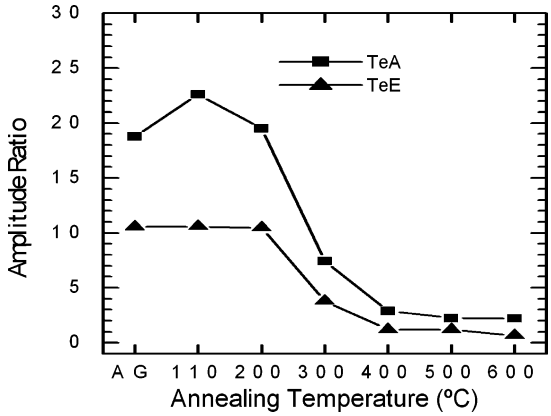

Figure 2. Raman Te A1 and E modes vs CdTe LO mode amplitude ratio.

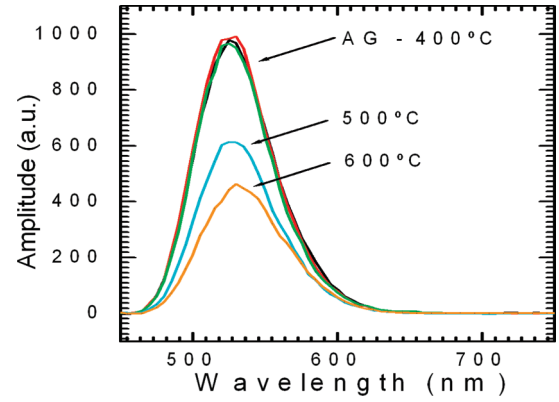

Figure 3. PL spectra of annealed and as-grown NPs. The spectra of the as-grown and 200, 300, and 400 °C annealed samples are overlapping and have thus been labeled together.

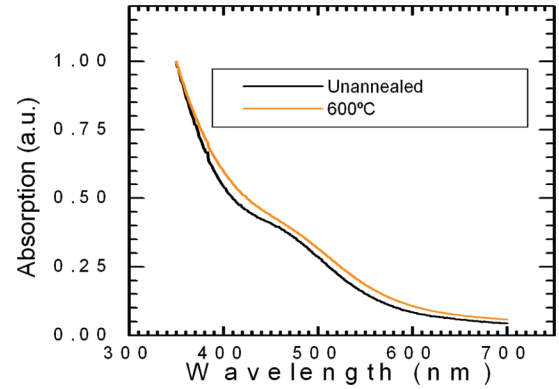

Figure 4. UV−vis absorption spectra of as-grown and 600 °C annealed samples.

in relation to the CdTe modes. When the Te A1 mode is compared to the CdTe LO mode, an intensity ratio of 19.52 is obtained in the 200 °C annealed sample, which decreases to a minimum of 2.20 in the 600 °C annealed sample. Similarly, the ratio between the Te E peak and the CdTe LO peak decreases in the same manner from 10.47 to 0.65. This intensity decrease of the Raman-active Te modes indicates the reduction in Te inclusions or surface defects within the NP and capping structure. What can be seen from the Raman scans is the progressive decrease in amplitude ratios between the Te and CdTe modes with increase of annealing temperature. The two control samples display identical characteristics, and when comparing these controls to both the 110 and the 200 °C annealed samples, no significant differences in the spectra could be identified. When the amplitude ratios are studied, there is little difference between control samples and those annealed at, or below, 200°. From inspecting the ratios at higher temperatures, it was observed that the amplitude ratios reduce by around 50% in the 300 °C and even further in the higher-temperature anneals. It is significant to note that the majority of the transition occurs with annealing temperatures between 200 and 400 °C, with insignificant change between as-grown and the 200 °C annealed sample nor with annealing temperatures above 400 °C. This leads to the conclusion that the annealing is affecting the NPs by reducing the Te inclusions or surface defects from the semiconductor core most dramatically between the temperatures of 200 and 400 °C. Increasing temperature while maintaining the constant annealing times progressively moves the samples further along in a crystallization mechanism, and thus, the aforementioned Raman peak ratios are obtained.

The PL results, which are shown in Figure 3, indicate that there is a reduction in PL intensity for samples annealed above 400 °C. This demonstrates that, for the annealing temperatures below 400 °C, the interface between the CdTe core and the capping ligands is not adversely affected. This is in high contrast to the effects of traditional annealing of semiconductor NPs in a polymer matrix, where PL reduction was observed at significantly lower-temperature (140 and 180 °C) anneals.[11] The PL is, however, reduced by a factor of 2 in the 600 °C annealed sample. The fact that the PL stays approximately constant at annealing temperatures below 400 °C in the RTA mechanism offers increased processing options in manufacturing and research. The observed reduction in PL intensity is attributed to an increase in the density of trapped states on the surface of the NPs, where nonradiative processes are dominant. This increase in density arises due to changes in interactions between the organic protecting layer and the CdTe NP surface. It is significant to note that the position and the shape of PL profiles were unchanged (a maximum red shift of ∼4 nm obtained for samples annealed at 600 °C). This indicates that the annealing does not significantly affect the size of CdTe NPs because the PL wavelength is subject to the quantum size effect and thus directly dependent on particle size. The UV-absorption scan shown in Figure 4 also corroborates the conclusion inferred from the PL about the size of the NPs, which were found not to change with increasing the annealing temperature. The unchanged PL peak also suggests that the polymer-capping layer is still intact even at a 600 °C annealing temperature. This fact is further verified by the ability to redisperse the NPs in water after annealing, which would be impossible if the polymer was carbonized and destroyed. What can also be seen from the figure is that, in the UV wavelength regime, the absorption curves are virtually identical. In this region, the absorption is dominated by the polymer structure, and as such, it is known that the polymer is not being degraded due to the processing. While there are some changes at the polymer/core interface attributing to the loss in PL intensity in the high- temperature anneals, the quantum confinement of these NPs and overall polymer structure are preserved in all samples. Utilizing an RTA process allows for much higher-temperature anneals in comparison to traditional annealing processes, without affecting the PL and maintaining an intact polymer-capped NP.

An insight into the structural features of these polymer-stabilized NPs was obtained from the transmission electron microscopy (TEM) images. TEM reveals CdTe NPs of nominally constant size, as is evident in Figure 5a taken from the unannealed sample. The NPs have a diameter on the order of 3−5 nm. Critical to any potential application of these CdTe

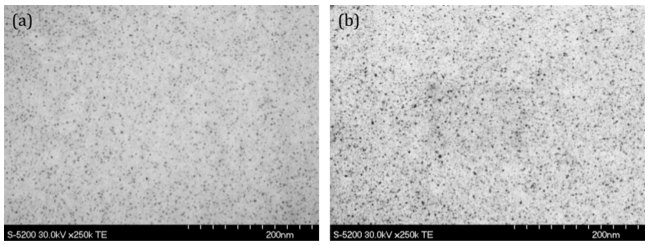

Figure 5. TEM image of the (a) as-grown sample and (b) 500 °C annealed sample.

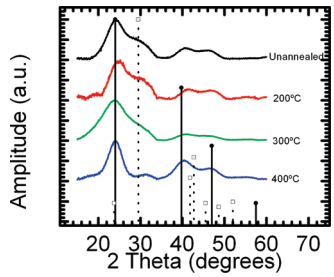

Figure 6. Overlay spectra of the XRD of the as-grown and 200, 300, and 400 °C annealed samples. Powder diffraction lines of wurzite (□) and zincblende (•)-type crystalline CdTe markers are shown as references.

NPs is their thermal and optical stability after exposure to thermal treatment. Figure 5b of the 500 °C annealed sample displays similar characteristics to the unannealed image. TEM was taken on all other temperature samples, and the size of the NPs remained constant. This finding is in contrast to an earlier finding by Dayal et al., wherein furnace-annealed CdTe NPs dispersed in SiO2 film grew in size.[29] Similarly, in another study, the size of aqueous grown CdTe NPs was also seen to increase with higher annealing temperatures, according to Bandaranyake et al., in a conventional annealing environment.[30] The fact that, under the RTA process, these CdTe NPs retain their initial size offers advantages for incorporating NP implementation into optoelectronic devices. This invariance of NP size, as seen from TEM, corroborates with the PL and UV-absorption results.

XRD measurements allow for identification of crystalline phases in the NPs; however, it is not as sensitive as the Raman technique to the relatively small changes that are taking place.[26] In Figure 6, the XRD results are shown along with the significant powder diffraction lines characteristic of wurzite and zincblende CdTe (pictured on the bottom of Figure 6 as square outlines and solid circles, respectively). Markers were taken from the powder diffraction files of zincblende (PDF # 01-075-2086) and wurzite (PDF # 01-080-0089). The XRD results display broad features with no sharp crystalline peaks, in contrast to what would be expected in bulk crystalline materials. The broadening is a result of the nanometer scale dimensions of the particles and is typical of other XRD results on NPs.[30] There are three peaks located at approximately 24°, 40°, and 46° that indicate the presence of a zincblende structure and correlate to reflections from the 111, 220, and 311 planes, respectively. However, another feature present most clearly in the unannealed and 200 °C annealed samples is a shoulder off of the 111 peak at around the 29° mark. This feature may be attributed to irregularities and randomization present in the crystal, which is characteristic of the synthesis procedure. It could also relate to the 102 plane found in a wurzite CdTe structure. Regardless of the uncertainty associated with this feature, the trend of the systematic reduction of the feature at 29° is evident from the XRD results. The reduction is consistent up to an annealing temperature of 400 °C, where it is no longer detectable. At this temperature, the XRD spectra clearly display a crystal structure of the zincblende form. This suggests that there are changes occurring in the NP core that cause the zincblende crystalline phase to prevail upon annealing at a sufficiently high annealing temperature. This conclusion corroborates previously documented research into the annealing of CdTe QDs, where the zincblende form of CdTe prevailed regardless of temperature.[30] In the 400 °C annealed sample, the XRD results show that the NP core has crystallized into a structure with features that correlate very closely to the zincblende markers combined with the reduction of the extraneous 29° feature beyond the detection limit. This crystalline reorganization occurs over the same temperature range in which the Raman mode ratios were seen to vary the greatest. The observed change can be attributed to one of two route causes. In the first reasoning, if it is assumed that the feature at 29° is a result of the 102 plane in wurzite CdTe, the RTA process above 200 °C acts to remove the wurzite form CdTe within the NP, thus reducing grain boundaries. This will, in turn, account for the trends seen in the XRD measurements and also the observed Raman mode ratio trends; less grain boundaries translate to a reduced number of surface defects between crystal phases, and hence, Te−Te bonds will subsequently be reduced. On the other hand, if the feature at 29° is attributed to randomization in the crystal due to the synthesis process, the RTA process serves to remove these crystal defects and randomization, as demonstrated through both the XRD spectra and the Raman mode ratio trends. In both cases, what is significant is the fact that the semiconductor core after the RTA process is displaying an enhanced level of crystallinity when compared with the as-grown NP. The XRD data reflects the crystalline changes that were identifiable using Raman spectroscopy, whereby the crystalline quality of the semiconductor core is improved. This improvement in the NP core can be vital to NP-based devices that rely on a high degree of NP core crystallinity.

X-ray photoelectron spectroscopy has also been utilized to analyze the chemical composition of NP surfaces before and after the rapid thermal annealing process. As a representative example, the main core-level features of as-grown and samples annealed at 300 °C are described. Figure 7a,d displays XPS high-resolution spectra of C1s of the as-grown sample and 300 °C annealed sample, respectively. The core-level C1s spectra of these samples is deconvoluted into three components with binding energies at 285.43, 286.36, and 288.37 eV, corresponding to carbons in different chemical environment, that is, C−C, (C)−C═O, and (O)−C═O, respectively. The O 1s core-level high-resolution spectra also demonstrate two deconvolved peaks at 532.41 and 533.81 eV. The intensity of the peak at higher binding energy (533.81 eV), which is attributed to the unbound (OH) groups of the organic polymer layer, decreases with annealing temperature, as expected. These peak components are specifically assigned to the PAA chains and hence imply the incorporation of a protective organic polymer layer onto the CdTe NP surface.[31] Depending on the extent of surface coverage, not only the composition of the NPs can be greatly affected but also their ability to prevent core oxidation. As depicted in Figure 7b,e, the peak at 572.63 is attributed to Te $3d_{5/2}$ in the form of CdTe and that of 575.95 to Te $3d_{3/2}$ in TeO_2.[32] The XPS shows trace amounts of Te oxides; however, its content cannot be seen from the elemental analysis. This suggests an insignificant amount of Te oxide present in samples annealed up to 600 °C, in contrast to the Te bonded with Cd. The presence of the Cd $3d_{5/2}$ peak at 405.56 eV and Cd $3d_{3/2}$ at

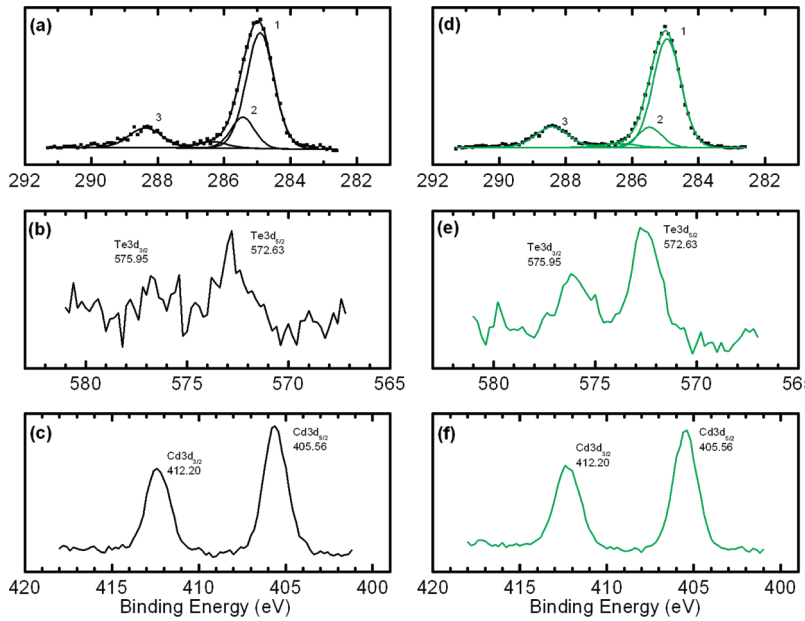

Figure 7. High-resolution XPS of C 1s scan of (a) as-grown samples and (d) 300 °C annealed sample: the peak labeled 1 is the C−C bond, the peak labeled 2 is the (C)−C═O bond, and the peak labeled 3 is the (O)−C═O bond. 3d Te scans of (b) as-grown samples and (e) 300 °C annealed sample. 3d Cd scans of (c) as-grown samples and (f) 300 °C annealed sample.

412.20, as shown in Figure 7c,f, clearly indicates that Cd exists in the form of CdTe.[32] No change in the shape or the position maxima of such deconvoluted peaks is observed during the thermal annealing, suggesting that Cd and Te are still bound together. As is evident from the XPS data, the RTA process does not induce any significant changes in the carbon, oxygen, Cd, and Te core-level features, suggesting that the overall composition of the NPs is still intact with minimal polymer degradation.

Conclusion

In conclusion, it was found that, through the RTA process, the semiconductor core of CdTe NPs can be influenced to develop a higher degree of crystallinity as compared with the unprocessed materials. This crystalline shift has been verified by both Raman spectroscopy in a HC-PCF liquid core waveguides and XRD scans. Combined with the tailoring of the crystalline core, the size of the NPs remains stable with temperature, in comparison to NPs that have undergone a traditional annealing process, where they were found to increase in size. The capping polymer remains intact and maintains the quantum confinement of the NPs up to an annealing temperature of 600 °C. The PL efficiency is nominally unaffected up to an annealing temperature of 400 °C, which is significantly higher than the glass-transition temperature of the PAA capping material. The overall features of the NPs, such as size, size dispersion, and aggregation behavior, were not altered after the exposure to RTA. The stability of the as-grown CdTe NPs has been repeatedly confirmed using PL and Raman spectroscopy. The most recent analysis took place nearly a year after the original synthesis date, and no change is evident in the characterization between the current material and the scans performed months ago. In addition, no detectable change in the optical properties of the thermally processed nanoparticles has been seen over the same duration. These findings also uncover a new route to optimizing the synthesis of water-soluble CdTe NPs with improved thermal and optical stability, which is an important goal for many applications.[33−35]

Acknowledgment. The Ontario Centre for Excellence (OCE) (Research Fund 72032825) is acknowledged for financial support. We would also like to thank Geoff Strause at Florida State University for help with the XRD measurements.

References and Notes

(1) Murray, B.; Kagan, C. R.; Bawendi, M. G. *Annu. Rev. Mater. Sci.* **2000**, *30*, 545.
(2) Bawendi, M. G.; Steigerwald, M. L.; Brus, L. E. *Annu. Rev. Phys. Chem.* **1990**, *41*, 477.
(3) Alivisatos, P. *Science* **1996**, *271*, 933.
(4) Somers, R. C.; Bawendi, M. G.; Nocera, D. C. *Chem. Soc. Rev.* **2007**, *36*, 579.
(5) (a) Bang, J. H.; Kamat, P. V. *ACS Nano* **2009**, *3*, 1467. (b) Anderson, I. E.; Breeze, A. J.; Olson, J. D.; Yang, L.; Sahoo, Y.; Carter, S. A. *Appl. Phys. Lett.* **2009**, *94*, 063101. (c) Gratzel, M. *Philos. Trans. R. Soc., A* **2007**, *365*, 993. (d) Lan, G. Y.; Yang, Z. S.; Lin, Y. W.; Lin., Z. H.; Liao, H. Y.; Chang, H. T. *J. Mater. Chem.* **2009**, *19*, 2349.
(6) Dooley, C. J.; Dimitrov, S. D.; Fiebig, T. *J. Phys. Chem. C* **2008**, *112*, 12074.
(7) Agarwal, A.; Lilly, G. D.; Govorov, A. O.; Kotov, N. A. *J. Phys. Chem. C* **2008**, *112*, 18314.
(8) (a) Fendler, J. H. *Chem. Mater.* **2001**, *13*, 3196. (b) Puntes, V. F.; Krishnan, K. M.; Alivisatos, A. P. *Science* **2001**, *291*, 2115.
(9) (a) Chan, W. C. W.; Nie, S. *Science* **1998**, *281*, 2016. (b) Tang, Z.; Wang, Y.; Podsiadlo, P.; Kotov, N. A. *Adv. Mater.* **2006**, *18*, 3203. (c) Zheng, Y.; Ying, J. Y. *Adv. Mater.* **2007**, *19*, 376.
(10) (a) Scholes, G. D. *Adv. Funct. Mater.* **2008**, *18*, 1157. (b) Fan, Z.; Razavi, H.; Do, J.-W.; Moriwaki, A.; Ergen, O.; Chueh, Y.-L.; Leu, P. W.; Ho, J. C.; Takahashi, T.; Reichertz, L.-A.; Neale, S.; Yu, K.; Wu, M.; Ager, J. W.; Jarvey, A. *Nat. Mater.* **2009**, *8*, 648. (d) Lin, W.; Frtitz, K.; Guerin, G.; Bardajee, G. R.; Hinds, S.; Sukhovatkin, V.; Sargent, E. H.; Scholes, G. D.; Winnik, M. A. *Langmuir* **2008**, *24*, 8215.
(11) Niu, Y.-H.; Munro, A. M.; Cheng, Y. J.; Tian, Y.; Liu, M. S.; Zhao, J.; Bardecker, J. A.; Plante, I. J.-L.; Ginger, D. S.; Jen, A. K.-Y. *Adv. Mater.* **2007**, *19*, 3371.
(12) Zhang, Y.; Zhang, H.; Ma, M.; Guo, X.; Wang, H. *Appl. Surf. Sci.* **2009**, *255*, 4747.
(13) Kalyuzhny, G.; Murray, R. W. *J. Phys. Chem. B* **2005**, *109*, 7012.
(14) Brandup, J., Immergut, E. H., Grulke, E. A., Eds. *Polymer Handbook*, 4th ed.; John Wiley & Sons: New York, 1999; Glass Transition Temperature of Polymers Online Table.
(15) Lee, T.; Park, O. O. *Adv. Mater.* **2000**, *12*, 801.
(16) (a) Roozeboom, F., Ed. *Advances in Rapid Thermal Annealing and Integrated Processing*; Nato ASI Series E: Applied Science; Kluwer Academic Publishers: Dordrecht, The Netherlands, 1996; Vol. 318. (b) Borisenko, V. E.; Hesketh, P. J. *Rapid Thermal Processing of Semiconductors*; Plenum Press: New York, 1996. (c) Fukuda, H., Ed. *Rapid Thermal*

Processing for Future Semiconductors; Elsevier: Amsterdam, The Netherlands, 2003; Proceedings of the 2001 International Conference on Rapid Thermal Processing, RTP 2001, Ise-Shima, Japan, 2001. (d) Singh, R. *J. Appl. Phys.* **1988**, *63*, R59.

(17) Bhattacharayya, D.; Helmy, A. S.; Bryce, A. C.; Avrutin, E. A.; Marsh, J. H. *J. Appl. Phys.* **2000**, *88*, 4619.

(18) Schaarschmidt, A.; Farah, A. A.; Aby, A.; Helmy, A. S. *J. Phys. Chem. B* **2009**, *113*, 9352.

(19) Kim, J.-S. K.; Friend, R. H. *Appl. Phys. Lett.* **2005**, *87*, 023506−1.

(20) Hikmet, R. A. M.; Chin, P. T. K.; Talapin, D. V.; Weller, H. *Adv. Mater.* **2005**, *17*, 1436.

(21) Yan, X.; Cui, Y.; He, Q.; Wang, K.; Li, J. *Chem. Mater.* **2008**, *20*, 1522.

(22) Sanchez-Gaytan, B. L.; Cui, W.; Kim, Y.; Mendez-Polanco, M. A.; Duncan, T. V.; Fryd, M.; Wayland, B. B.; Park, S. *Angew. Chem., Int. Ed.* **2007**, *46*, 9235.

(23) Bardelang, D.; Zaman Md., B.; Moudrakovski, I. L.; Pawsey, S.; Margeson, J. C.; Wang, D.; Wu, X.; Ripmeester, J. A.; Ratcliffe, C. I.; Yu, K. *Adv. Mater.* **2008**, *20*, 4517.

(24) Irizar, J.; Dinglasan, J.; Goh, J. B.; Khetani, A.; Anis, H.; Anderson, D.; Goh, C.; Helmy, A. S. *IEEE J. Sel. Top. Quantum Electron.* **2008**, *14*, 1214.

(25) Ochoa, O.; Witkowski, E., III; Colajacomo, C.; Simmons, J.; Potter, B, Jr. *J. Mater. Sci. Lett.* **1997**, *16*, 613.

(26) Morell, G.; Reynés-Figueroa, A.; Katiyar, R.; Farias, M.; Espinoza-Beltran, F.; Zelaya-Angel, O.; Sánchez-Zinencio, F. *J. Raman Spectrosc.* **1994**, *25*, 203.

(27) Vinogradov, V. S.; Karczewski, G.; Kucherenko, I. V.; Mel'nik, N. N.; Fernadez, P. *Phys. Solid State* **2008**, *50*, 164.

(28) Caballero-Briones, F.; Zapata-Navarro, A.; Martel, A.; Iribarren, A.; Peña, J. L.; Castro-Rodríguez, R.; Bartolo-Pérez, P.; Rábago-Bernal, F.; Jiménez-Sandoval, S. *Superfices y Vacio* **2003**, *16*, 38.

(29) Dayal, P. B.; Mehta, B. R.; Shivaprasad, S. M. *Jpn. J. Appl. Phys.* **2005**, *44*, 8222.

(30) Bandaranayake, R. J.; Wen, G. W.; Lin, J. Y.; Jiang, H. X.; Sorenson, C. M. *Appl. Phys. Lett.* **1995**, *6*, 831.

(31) Beamson, G.; Briggs, D. *High Resolution XPS of Organic Polymers. The Scienta ESCA 300 Database*; John Wiley & Sons: Chichester, U.K., 1992; p 110.

(32) Etcheberry, A.; Iranzo-marin, F.; Novakovic, E.; Triboulet, R.; Debiemme-Chouvy, C. *J. Cryst. Growth* **1998**, *184/185*, 213.

(33) Neretina, S.; Sochinskii, N. V.; Mascher, P. *J. Electron. Mater.* **2005**, *34*, 786.

(34) Lee, H. S.; Lee, K. H.; Kim, J. S.; Park, H. L. *J. Mater. Sci.* **2004**, *39*, 7115.

(35) Ramirez-Bon, R.; Espinoza-Beltran, F. J.; Arizpe-Chavez, H.; Zebya-Angel, O.; Sanchez-Sinencio, F. *J. Appl. Phys.* **1995**, *77*, 5461.

JP9079475